Journal of Materials Chemistry C

ROYAL SOCIETY OF CHEMISTRY

PAPER

View Article Online
View Journal

Cite this: DOI: 10.1039/d0tc02558e

Highly conductive wet-spun PEDOT:PSS fibers for applications in electronic textiles†

Ruben Sarabia-Riquelme, *[a] Rodney Andrews,[a] John E. Anthony [b] and Matthew C. Weisenberger[a]

Received 28th May 2020,
Accepted 27th July 2020

DOI: 10.1039/d0tc02558e

rsc.li/materials-c

The emerging field of electronic textiles is currently hindered by a lack of mechanically robust fibers and yarns that efficiently conduct electricity. Conjugated polymer fibers are promising candidates to meet those requirements. In this work, a wet-spinning process is described to fabricate PEDOT:PSS fibers with electrical conductivities up to 3663 ± 326 S cm^{-1}, Young's moduli up to 22 GPa and tensile strength of 550 MPa, through inclusion of a sulfuric acid drawing step. The mechanism by which the sulfuric acid drawing step enhances the electrical and mechanical properties of the fibers is investigated. Moreover, the electrical conductivity of these fibers was further increased to 4039 ± 215 S cm^{-1} by immersing the fibers in sulfuric acid for additional time, at the expense, however, of lowering their Young's modulus and tensile strength. Additionally, we demonstrate the use of the fibers in various electronic textile applications such as: (a) flexible textile interconnections in an LED circuit, (b) a proof of concept thermochromic fiber bundle that changes color on demand, (c) a thermoelectric textile device using the fibers as the p-type legs, and (d) using the fibers as the channel in an organic electrochemical transistor to build an LED dimmer. This work presents a unique type of material with the potential of becoming a cornerstone in the emerging field of electronic textiles.

1. Introduction

The first evidence of textiles dates back to around 41 000 to 52 000 years ago. A 3-ply cord made from inner bark fibers was found in southern France suggesting that Neanderthals already possessed fiber technology.[1] Moreover, woven materials were found in Pavlov, Czech Republic dating to *a.* 26 000 years ago.[2] However, despite the technological advancements in other areas, textiles have remained relatively unmodified. Although miniaturization of electronic devices and circuits have allowed them to be embedded in traditional textiles,[3] the fiber technology itself has not changed. In future electronic textiles, instead of embedding electronic devices into textiles, ideally the constituent fiber itself will have electronic capabilities so that these "electronic fibers" can function as building blocks and be arranged into woven patterns to construct fiber-based devices. However, to realize this idea, new fibers and yarns that are electrically conductive and mechanically robust are needed.

Conjugated polymers are great candidate materials to fabricate such electronic fibers because they are comprised of earth-abundant, inexpensive elements, have good mechanical properties and flexibility, and conduct electricity well. Currently, the primary method to fabricate electrically conductive fibers from conjugated polymers is to deposit or coat them onto an inert fiber support such as the *in situ* polymerization of polypyrrole and poly(3,4-ethylenedioxythiophene) (PEDOT) on silk fiber,[4] cotton,[5] wool,[6] and polyester fabric.[6,7] By itself, PEDOT is an insoluble polymer. However, PEDOT complexed with the counterion poly(styrenesulfonate) (PSS), or PEDOT:PSS, can form stable water dispersions, which have been widely used to dye textile fibers such as nylon,[8] polyester,[9] cotton,[10] or silk.[11,12] In these fibers, the insulating core fiber acts as load-bearing support, ensuring robust mechanical properties while the conjugated polymer coating provides for electrical conduction. However, the volume occupied by the thin conjugated polymer coating is typically very small compared to the volume of insulating fiber. Thus, the bulk electrical conductivity of these coated textiles is usually small, often lower than 10 S cm^{-1}, limiting their applications.[13]

Direct spinning of conducting polymers into fibers has been explored to circumvent these limitations. Polyaniline was the first conducting polymer to be spun into fibers using wet-spinning methods,[14–17] shortly followed by the spinning of other conducting polymers such as poly(3-alkyl-thiophenes),[18–20] and polypyrrole.[21–23] By virtue of the water dispersibility of PEDOT:PSS imparted by the counterion PSS, wet-spinning of

[a] *Center for Applied Energy Research, University of Kentucky, Lexington, Kentucky 40511, USA. E-mail: ruben.sarabia@uky.edu*
[b] *Department of Chemistry, University of Kentucky, Lexington, Kentucky 40506, USA*

† Electronic supplementary information (ESI) available. See DOI: 10.1039/d0tc02558e

PEDOT:PSS into fibers has also been possible.[24–32] Among the conjugated polymer fibers, the PEDOT:PSS fibers have shown the most promising properties with electrical conductivities as high as 3828 S cm^{-1}.[29] This value of electrical conductivity was achieved by extruding a water dispersion of PEDOT:PSS into a concentrated sulfuric acid coagulation bath with a residence time of 10 min. The high electrical conductivity of the fibers was attributed to the removal of excess insulating PSS in the concentrated sulfuric acid bath. The Young's modulus and break stress of these sulfuric acid spun fibers were 3.9 GPa and 425 MPa, respectively. Recently, our group reported the fabrication of highly oriented PEDOT:PSS fibers with maximum break stresses of 425 MPa and Young's moduli as high as 15.5 GPa.[30] These fibers were fabricated by continuous wet-spinning process of a PEDOT:PSS water dispersion into an isopropanol (IPA) coagulation bath and subsequent draw in a dimethylsulfoxide (DMSO) bath. The values of Young's moduli obtained were relatively high compared to previously reported PEDOT:PSS fibers and were attributed to the high degree of preferential orientation imparted to the polymer chains by drawing the fibers in DMSO. Nevertheless, the electrical conductivities of these DMSO-drawn fibers (between 1000–2200 S cm^{-1}) were somewhat lower than the sulfuric acid coagulated fibers (3828 S cm^{-1}).

The use of acids, particularly of sulfuric acid, to increase the electrical conductivity of PEDOT films is a common practice in the literature.[33–37] In fact, the highest electrical conductivity reported to date for a PEDOT:PSS film (4380 S cm^{-1}) was obtained by post-treating films with concentrated sulfuric acid.[35] Nevertheless, the exact mechanism by which sulfuric acid enhances the electrical conductivity of PEDOT:PSS materials (fiber or film) is still a topic of discussion. While most authors agree on the effectiveness of sulfuric acid to remove excess PSS, it is not clear whether sulfates partially substitute PSS as counterions. For instance, Xia *et al.* reported FTIR data that suggested the presence of sulfate ions in the structure of the sulfuric acid treated PEDOT:PSS films,[34] but Kim *et al.* dismissed this possibility suggesting that sulfuric acid only served as a very good solvent for PSS.[35] Furthermore, few reports exist that discuss the effect of these acid treatments on the mechanical properties of the material.

Motivated by this, we decided to explore the use of sulfuric acid (instead of DMSO) as a drawing media during the fabrication of PEDOT:PSS fibers, and elucidate its impact on the electrical and mechanical properties of the fibers. In general, sulfuric acid drawing improved the fiber properties, yielding values of electrical conductivity as high as 4039 ± 215 S cm^{-1}, Young's modulus of up to 22 GPa and break stress of approximately 550 MPa. These values are the highest reported to date for PEDOT:PSS fibers. Moreover, the structure and composition of the fibers after sulfuric acid drawing was studied using wide-angle X-ray scattering (WAXS) and X-ray photoelectron spectroscopy (XPS) to gain insight into the mechanism behind these improvements. It was found that sulfuric acid drawing not only induced a high degree of preferential orientation on the polymer chains, but also very effectively removed excess PSS from the fibers while promoting the substitution of PSS by sulfates as counterions. The partial removal of PSS and substitution of counterions led to a reorganization of the crystal structure of the fibers into forms more favorable for charge transport. Finally, various applications of the fibers in electronic textiles were demonstrated. These applications include the use of the fibers as flexible textile interconnections, thermochromic textiles, thermoelectric textiles, and as the channel in organic electrochemical transistors.

2. Experimental

2.1. Dope preparation

PEDOT:PSS water dispersion was purchased from Heraeus (PH1000; PEDOT : PSS weight ratio 1 : 2.5 (28.57 wt% PEDOT), solid content 1.3 wt%). The PEDOT:PSS dispersion was concentrated to 2.5 wt% by placing it on a hot plate at 90 °C and evaporating water. Afterward, 5 wt% of DMSO was added (with respect to the total solution) and the dope was further stirred for 2 h at room temperature. Then, the dope was bath sonicated for 30 min and finally degassed in a vacuum oven for 5 min at room temperature.

2.2. Fabrication of the fibers by wet-spinning

Table 1 summarizes the different fiber samples studied in this work. Raw fibers and DMSO-drawn fibers were fabricated following a procedure previously reported.[30] Briefly, the degassed PEDOT:PSS dope was transferred to a 5 mL syringe and placed in a syringe pump (KD Scientific) that kept the flow rate constant at 0.25 mL h^{-1}. The dope was extruded through a sintered metal disk filter (average pore size 5 μm) and exited through a 100 μm diameter capillary spinneret (length to diameter of the capillary of 5) into a coagulation bath of 10 vol% DMSO in IPA.

Table 1 Summary of the different samples studied in this work

		Post-coagulation drawing		
Sample name	Description	DMSO	H_2SO_4	Post-treatment
Raw fiber	Collected immediately after extrusion into coagulation bath	No	No	No
H_2SO_4-immersed	Raw fiber post-treated by immersion in 93 wt% H_2SO_4 for 1 to 60 min	No	No	Immersion in 93 wt% H_2SO_4 for 1 to 60 min
DMSO-drawn	Raw fiber drawn in pure DMSO after coagulation	Yes	No	No
H_2SO_4-drawn	Raw fiber drawn in 93 wt% H_2SO_4 after coagulation	No	Yes	No
H_2SO_4-drawn + immersed	H_2SO_4-drawn fiber post-treated by immersion in 93 wt% H_2SO_4 for 30 min	No	Yes	Immersion in 93 wt% H_2SO_4 for 30 min

After coagulation, the fiber was dried through an in-line heater in air at ~120 °C, prior to the first roller. After coagulation and drying, raw fibers could be recovered directly or further processed. In the case of DMSO-drawn fibers, the raw fiber subsequently entered a DMSO drawing bath followed by second in-line drying step through a keyhole-cylinder-shaped oven with a maximum air temperature of 170 °C before being taken-up on a spool. In the case of H_2SO_4-drawn fibers, the raw fiber entered a Teflon bath filled with 93 wt% sulfuric acid instead of the DMSO draw bath. Then, it entered a deionized water wash bath, and finally, was taken-up on a spool. In all cases, the total draw of each sample was calculated as the ratio between the take-up linear speed and the dope extrudate speed. H_2SO_4-immersed fibers were fabricated by immersing spools of raw fibers in 93 wt% sulfuric acid for different periods of time (between 1 and 60 min) at room temperature. Then, they were transferred to a deionized water bath for 10 min, and lastly, dried in an oven at 140 °C for 10 min. For comparison purposes, one spool of H_2SO_4-drawn fibers was also subjected to sulfuric acid immersion for 30 min. This sample is called H_2SO_4-drawn + immersed. All baths used were kept at room temperature.

2.3. Characterization of the fibers

To measure the electrical conductivity, five fiber specimens per each sample (having each a different length of 1, 2, 3, 4 and 5 cm) were laid between two copper strips and contacted using silver paint. Then, the resistance was measured using a Keithley 2100 microvoltmeter. The contact resistance could be extracted from resistance *versus* length plots, but it was found to be $<5\%$ in all cases. The electrical conductivity was calculated from the measured resistance, length, and cross-sectional area of each specimen. The values presented in this work are the average value of the five specimens while the error bars represent the standard deviation.

Scanning electron microscope imaging of the fibers was performed on a Hitachi S-4800 field emission SEM at 10 kV accelerating voltage and 10 μA beam current. Gold sputtering was not necessary. Typically, the five fiber specimens used to measure electrical conductivity were placed in the SEM to obtain their average diameter. For each specimen 10 diameter values were measured at different points along the specimen, giving a total of 50 measured values per sample. The average value was taken as the average diameter of the sample and error bars represent the standard deviation.

Mechanical testing was performed on at least five fiber specimens per sample in uniaxial tension using the single-fiber test system, FAVIMAT+ from Textechno. The pretension was 0.50 cN per tex with a test speed of 5 mm min^{-1} over a gauge length of 25.4 mm (*i.e.* 1 inch). Values presented in this work are average values and error bars represent standard deviation. The FAVIMAT+ system was also used to measure the average linear density of each specimen tested using an ultrasonic resonance method.

Wide-angle X-ray Scattering experiments were performed in transmission mode using the Xenocs Xeuss 2.0 SAXS/WAXS system located at the Electron Microscopy Center of the University of Kentucky. The source was GeniX3D Cu ULD 8 keV with wavelength of 1.54 Å. Typically, several fibers were aligned into a bundle and placed on an aperture card. The aperture card was then transferred to the WAXS sample holder and placed at 101.17 mm from the 2D detector (Dectris Pilatus 200 K). Exposure time was 600 s. Data processing was performed using the software Foxtrot provided by Xenocs.

X-ray photoelectron spectroscopy was performed using the K-Alpha XPS (Thermo Scientific) with A1 Kα X-ray monochromator from the Electron Microscope Center of the University of Kentucky to obtain the XPS spectra of PEDOT:PSS fiber bundles placed on an aperture card. The software Avantage provided by Thermo Scientific was used to analyze the data.

To fabricate the thermochromic bundle, a turquoise blue to clear thermochromic pigment with a switching temperature of 31 °C was purchased from Uniglow Products. The pigment was mixed with titanium white acrylic paint from Artist's Loft to obtain a thermochromic acrylic based paint that changed from blue to white at 31 °C. A bundle of DMSO-drawn fibers was dipped in the paint and left to dry overnight at room temperature.

To fabricate the organic electrochemical transistors, DMSO-drawn fibers were used as the channel and copper wire as the gate. The solid polymer electrolyte was fabricated by adding polyvinyl alcohol (PVA) (5 g, average molecular weight 95 000, Acros Organics) and 85% phosphoric acid (5.88 g) to deionized water (40 g) and stirring on a hot plate at 90 °C until a clear solution was obtained. Then, a drop of the solution was placed on top of the copper wire and PEDOT:PSS fiber and left to dry overnight.

3. Results and discussion

3.1. Sulfuric acid immersion tests

As a first test to observe the effects that sulfuric acid might have on the fibers, spools of raw fibers with electrical conductivities around 1000 S cm^{-1}, were immersed in 93 wt% sulfuric acid for different periods of time (between 1 and 60 min) at room temperature (see Experimental section for more details). These fibers are called H_2SO_4-immersed. Fig. S1a and b (ESI†) show an immediate reduction in diameter and linear density, respectively, for two sets of samples (with two different coagulation bath draw ratios of 1.58 and 3.34) within one minute of sulfuric acid treatment. Further immersion times resulted in little additional change in these values. However, the electrical conductivity of the H_2SO_4-immersed fibers increased with increasing treatment time until stabilizing after ~30 min at values around 3200–3500 S cm^{-1} (see Fig. S1c, ESI†).

3.2. Design of an in-line sulfuric acid drawing step

In view of the positive results obtained from the sulfuric acid immersion tests, an in-line sulfuric acid drawing step was designed. Here, the DMSO draw bath was substituted by a 93 wt% sulfuric acid draw bath followed by a deionized water wash bath. The hypothesis was that higher electrical conductivities

would be attained by performing the sulfuric acid treatment while drawing the fiber and inducing preferred orientation. Fig. S2a (ESI†) shows a scheme of the wet-spinning process including these modifications. Here, the fiber speed was adjusted such that the residence time of the fiber in the sulfuric acid bath was approximately 1 min while the total draw ratio (ratio between take-up speed and dope extrudate speed) was typically between 1.8 and 2.4. Tens-of-meters long spools of H_2SO_4-drawn fiber were obtained using this method. For comparison purposes, one spool of H_2SO_4-drawn fibers was also subjected to sulfuric acid immersion for 30 min. This sample is called H_2SO_4-drawn + immersed. Fig. S2b–d (ESI†) show SEM images of the different types of fibers. In all cases, cylindrical-shaped high-quality fibers with smooth surfaces were obtained.

3.3. Linear density and XPS analysis of the fibers

Fig. 1a plots the linear density of raw fibers, DMSO-drawn, H_2SO_4-immersed, H_2SO_4-drawn and H_2SO_4-drawn + immersed fibers as a function of total draw. The dotted curves are calculated using eqn (S4) (ESI†) and indicate the predicted linear density of a fiber for a certain weight percentage of PEDOT in the final fiber (see Discussion in the ESI†). As can be observed, the raw fibers are close to the 28.57 wt% PEDOT curve, which corresponds to the wt% PEDOT to PSS from the manufacturer. The DMSO-drawn fibers are enriched in PEDOT, with linear densities in the 35–40 wt% PEDOT range. And the sulfuric acid treated fibers (drawn and/or immersed) are richer still in PEDOT, 60–70 wt% range. These results indicate that there is removal of excess PSS from the fibers during DMSO and sulfuric acid drawing. Furthermore, they suggest that sulfuric acid is more efficient in removing excess PSS from the fibers than DMSO, similar to other reports.[34,35] The diameters of the fibers (Fig. 1b) decrease as a function of total draw. Additionally, as a result of loss of PSS, the sulfuric acid treated fibers had the smallest diameters, followed by the DMSO-drawn fibers, and then, raw fibers.

To gain further insight into the compositional changes occurring in the fibers as a result of the different treatments, XPS was performed on bundles of raw fibers, DMSO-drawn fibers, H_2SO_4-drawn fibers, and H_2SO_4-drawn + immersed fibers. Fig. 1c shows the C1s XPS scans of the four samples. The curves can be deconvoluted into three components; the sp^3 and sp^2 carbon–carbon bonding appear at ~284.8 eV, the carbon–oxygen and carbon–sulfur bonds appear as a broader peak at ~286 eV (in interest of simplicity, we do not attempt to deconvolute this signal into two separate contributions), and the carbon–oxygen double bonds appear around 289 eV.[38,39] The intensity of the C–O/C–S peak slightly increases after the DMSO drawing and increases more notably after the sulfuric acid treatments. The area ratio between the C–O/C–S peak and the C–C/C=C peak is 0.44 for the raw fibers, 0.55 for the DMSO-drawn fibers, 1.08 for the H_2SO_4-drawn fibers and 1.11 for H_2SO_4-drawn + immersed fibers. If we consider the chemical structures of PEDOT and PSS, the ratio of C–O/C–S bonds to C–C/C=C bonds for PEDOT and PSS is 1.33 and 0.11, respectively. Therefore, the increase of this ratio indicates an increase in the concentration of PEDOT with respect to PSS (due to loss of PSS in DMSO and acid bath treatments). The increase in PEDOT concentration is larger in the sulfuric acid treatments, which is consistent with the linear density results. The small peak at 289 eV could stem from C=O bonds present in some of the resonance structures of PEDOT, which explains its increase with increasing PEDOT concentration.

The S2p XPS scans for the same four samples are presented in Fig. 1d. The S2p line of PEDOT:PSS is typically deconvoluted into two doublets ($Sp_{1/2,3/2}$) corresponding to the two distinct

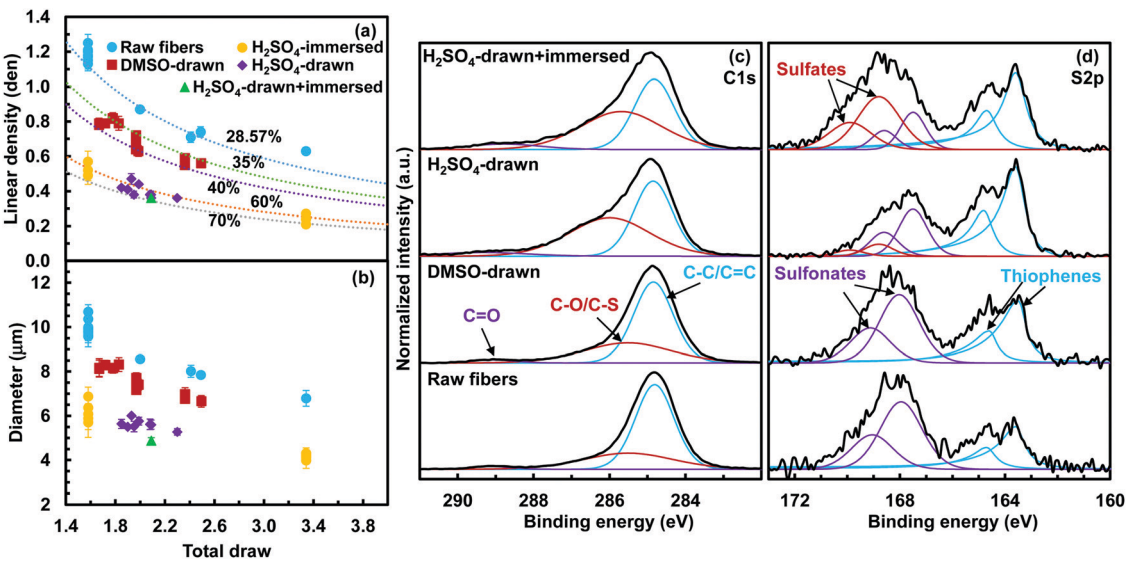

Fig. 1 (a) Linear density of the fibers as a function of total draw. The linear density is given in units of denier, which correspond to grams per 9000 m of a fiber. The dotted curves represent the linear density of the fibers as calculated from a mass balance (eqn (S4), ESI†) using the noted wt% of PEDOT in the final fiber. (b) Average diameter of the fibers as a function of total draw. XPS spectra of the fibers. (c) C1s scan and (b) S2p scan. Intensities are normalized to the maximum intensity.

chemical states of sulfur encountered in PEDOT:PSS, *i.e.* thiophene and sulfonate. The thiophene doublet appears at ~163.6 and 164.7 eV[36,39–41] with an asymmetric tail that extends into higher binding energies due to the positive charge in the oxidized PEDOT chain that gets partially localized on the sulfur atoms.[40,42] The sulfonate component is found at higher binding energies, around 168 eV.[40,43] While the intensity of the thiophene doublet increases with respect to the sulfonate doublet after drawing the fibers through DMSO, consistent with partial removal of PSS from the fibers in the DMSO bath, the increase in intensity of the thiophene doublet is substantially more pronounced after drawing the fibers through sulfuric acid. The data support the results obtained from the C1s scans and suggests, as did the linear density studies, that drawing in sulfuric acid is more effective at removing PSS from the fibers than in DMSO. In addition to the increase in intensity of the thiophene doublet, we also note that the sulfonate doublet shifts towards lower binding energies. The sulfonate signal actually has two components. One component is the sulfonic acid group $SO_3^-H^+$ and the other is the sulfonate group acting as counterion for PEDOT, $SO_3^-PEDOT^+$.[40] The sulfonic acid component appears at higher binding energies, therefore, the shift towards lower binding energy indicates a decrease of this component with respect to the sulfonates acting as counterions. The commercial PEDOT:PSS dispersion used in this work contains excess PSS (PEDOT : PSS weight ratio 1 : 2.5). Therefore, in the raw fibers, most of the sulfonate groups are in the $SO_3^-H^+$ form. DMSO is only partially effective at removing PSS and thus, the $SO_3^-H^+$ form remains as the majority after DMSO draw. However, upon treatment with sulfuric acid, significantly more excess PSS is washed off and the sulfonate groups acting as counterions become the majority, shifting the signal towards lower binding energies. Moreover, after drawing in sulfuric acid, an additional doublet appears at higher binding energies (168.8 eV), and increases in intensity upon further immersing the fibers in sulfuric acid for 30 min. This doublet indicates the presence of sulfates in the fibers after sulfuric acid treatment.[36,39,41] Therefore, sulfuric acid treatment not only removes excess PSS from the fibers, but it also leads to partial substitution of PSS with sulfates as counterions. This finding is consistent with the findings of others[34,36] who also observed indications of sulfate groups remaining in the structure after sulfuric acid treatment. Note that the sulfate signal could also be partially stemming from residual sulfuric acid remaining in the fibers despite thoroughly washing with excess water.

3.4. WAXS analysis and proposed changes on the crystal structure of the fibers

Fig. 2a–d show the 2D WAXS patterns of raw fibers, DMSO-drawn fibers, H_2SO_4-drawn fibers, and H_2SO_4-drawn + immersed fibers, respectively. In all cases, characteristic arcs indicating preferred orientation of the crystallites along the fiber axis were observed. The integrated intensity *versus* 2θ is presented in Fig. 2e. Three distinct features can be differentiated for all samples. First, the broad hump at approximately 18° is attributed to amorphous and randomly oriented PSS.[30,44,45] This broad hump decreases in intensity after the fibers have been drawn in DMSO and is practically non-existent for the fibers that have been treated with sulfuric acid, due to the removal of the majority of the PSS. Second, the peak at approximately 26.2° is assigned to the PEDOT (020) reflection, corresponding to the π–π stacking of PEDOT chains (*b*-direction in Fig. 2f) with a π–π stacking distance of 3.4 Å.[35,44,46,47] Finally, the feature appearing at small angles between 3° and 8° is assigned to the PEDOT (100) reflection, which corresponds to the lamella stacking of PEDOT and counterion (*a*-direction in Fig. 2f). In the case of raw fibers and DMSO-drawn fibers, the (100) peak is found at 3.7° which corresponds to a *d*-spacing of 23.6 Å. This peak shifts toward larger angles and splits into two peaks after the fibers have been drawn in sulfuric acid. In that case, the two peaks are found at 4.8° and 6.6°, which correspond to *d*-spacings of 18.6 and 13.4 Å, respectively. Lastly, when the H_2SO_4-drawn fibers are additionally immersed in sulfuric acid for 30 min, the peak at 4.8° disappears and only the peak at 6.6° is observed. The small peak appearing between 10° and 13° is assigned to the second order reflection of the (100) peak as it follows accordingly the shifts described above.

The shifts in 2θ of the (100) peak indicate changes in the crystal structure of PEDOT and must be related to changes in the way PEDOT and counterions stack. A scheme with the proposed structural changes is shown in Fig. 2g. In the case of the raw fibers and DMSO-drawn fibers, the *d*-spacing of 23.6 Å is close to the sum of the theoretical widths of PEDOT and PSS (7.5 Å and 15.5 Å), and it corresponds to the alternate stacking of PEDOT and PSS, where PSS has its sulfonate groups oriented in the *a*-direction (Fig. 2g left).[48] The reduction of the (100) *d*-spacing from 23.6 Å to 18.6 Å in the H_2SO_4-drawn fibers could be related to a change in how PSS is accommodated in the structure, for example, with the sulfonate groups oriented in the *b*-direction instead of the *a*-direction as shown in Fig. 2g top right. This structure is similar to the stacking of PEDOT and tosylate anions (edge to face) with a (100) *d*-spacing of ~14 Å,[46] however, the bulkiness of the PSS counterion results in a larger distance in this case. Furthermore, the appearance of a second peak with (100) *d*-spacing of 13.4 Å after the sulfuric acid treatment is very interesting because similar values of *d*-spacing have been reported before for PEDOT with sulfate as counterion.[36,41,47,49] Therefore, the appearance of this peak is in line with some fraction of PSS being substituted by sulfate as the counterion (Fig. 2g bottom right). Thus, the H_2SO_4-drawn fibers show a mix of PEDOT-PSS and PEDOT-sulfate lamella stacking, yielding the split peak observed in the WAXS pattern. Further treating the fibers by immersing them in sulfuric acid for 30 min, promotes the reorganization of the remaining PEDOT chains still stacked with PSS to stack with sulfate anions instead, resulting in the disappearance of the peak at 4.8° and the increase in intensity of the peak at 6.6°. These results are also consistent with the increase in the intensity of the sulfate doublet relative to the sulfonate doublet in the XPS S2p scan (Fig. 1d).

The crystallite size along the *a* and *b* directions (L_a and L_b, respectively) was calculated using the Scherrer's equation (eqn (S5), ESI†). The values obtained are listed in Table 2.

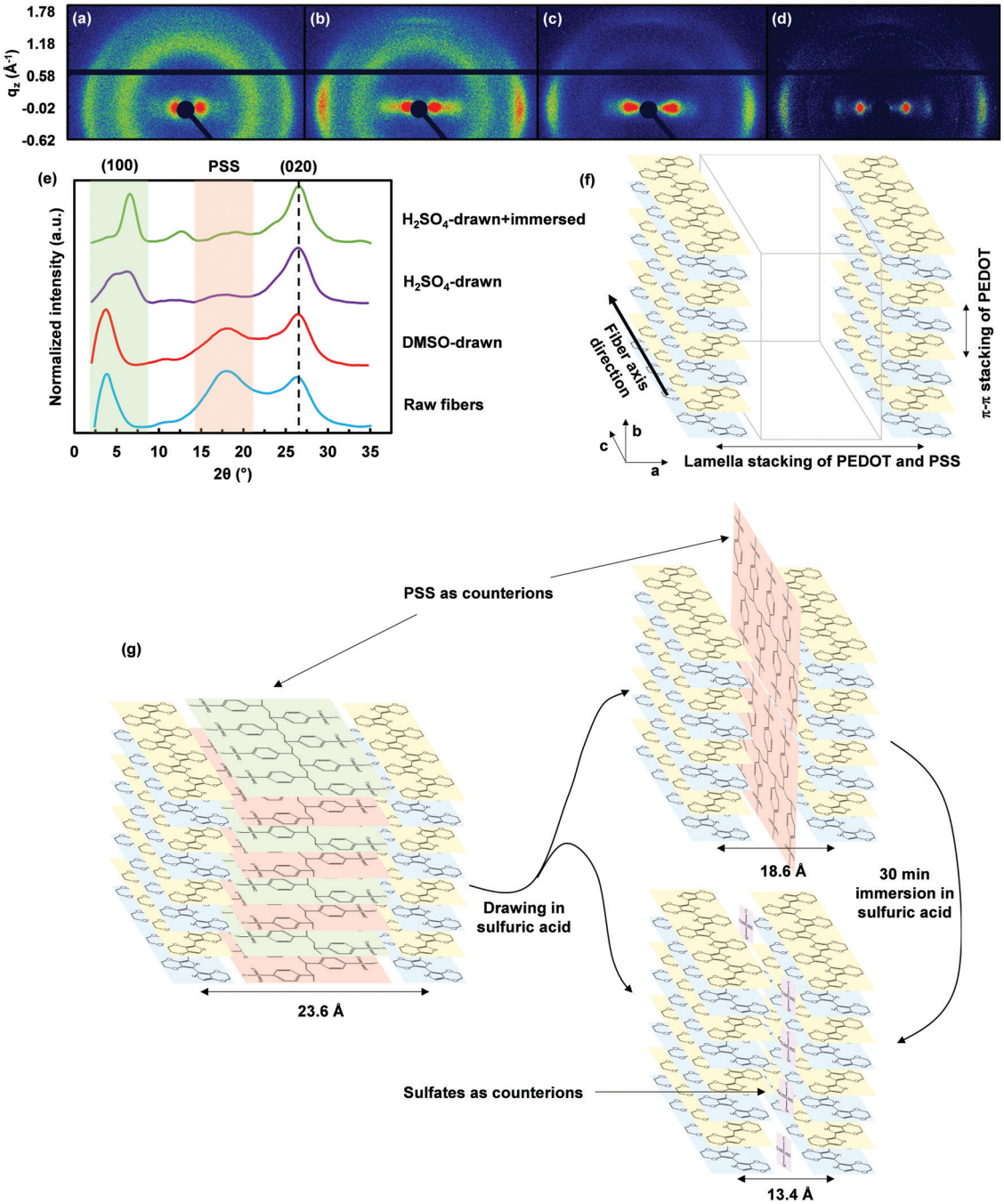

Fig. 2 WAXS analysis of PEDOT:PSS fibers. 2D WAXS patterns of (a) raw fibers, (b) DMSO-drawn fibers, (c) H_2SO_4-drawn fibers and (d) H_2SO_4-drawn + immersed fibers. (e) Integrated intensity (normalized to the maximum intensity) *versus* 2θ. (f) Scheme of the PEDOT crystal structure. (g) Scheme showing the proposed changes to the crystal structure PEDOT after sulfuric acid treatment.

L_a was found to be the same (around 35 Å) for both raw fibers and DMSO-drawn fibers. In the case of the H_2SO_4-drawn fibers, the crystallite size calculated from the (100) lamella stacking of PEDOT and PSS ($L_{a,\mathrm{PSS}}$) decreases to 27 Å, although the size calculated using the (100) lamella stacking of PEDOT and sulfates ($L_{a,\mathrm{sulfate}}$) has a higher value of 40 Å. Moreover, after immersing the fiber in sulfuric acid for 30 min, the peak corresponding to the lamella stacking of PEDOT and PSS disappears, and $L_{a,\mathrm{sulfate}}$ increases to 48 Å. L_b calculated from the (020) reflection was found to increase from 18 Å to 22 Å after DMSO drawing or sulfuric acid drawing, and to further increase to 25 Å after being drawn and immersed in sulfuric acid for 30 min. Therefore, the substitution of PSS by sulfate as a counterion seems to promote a more crystalline structure, given the increased crystallite sizes observed in both the *a* and *b* directions. This is likely due to reduced steric effects imposed in the structure by the smaller size sulfate counterions as opposed to the bulky PSS polymer chains. Using L_b and the

Table 2 Crystallite size in the *a* and *b* directions, number of PEDOT chains π–π stacked in the *b*-direction, and degree of crystallinity for the different fiber samples

Sample	$L_{a,\mathrm{PSS}}$ (Å)	$L_{a,\mathrm{sulfate}}$ (Å)	L_b (Å)	N	χ_c (%)
Raw fibers	35	—	18	5–6	49
DMSO-drawn fibers	35	—	22	6–7	56
H_2SO_4-drawn fibers	27	40	22	6–7	86
H_2SO_4-drawn + immersed fibers	—	48	25	7–8	83

π–π stacking distance of 3.4 Å, the number of PEDOT chains π–π stacked in the *b*-direction, *N*, can be estimated (Table 2), and is found to lie in the range of 5–6 PEDOT chains for raw fibers, increases to 6–7 for DMSO-drawn and H_2SO_4-drawn fibers, and increases further to 7–8 for H_2SO_4-drawn + immersed fibers.

Additionally, the degree of crystallinity, χ_c, was also calculated for the different samples (eqn (S6), ESI†). As can be observed in Table 2, the crystallinity of the samples increased from 49% to 56% after DMSO drawing. Nevertheless, H_2SO_4-drawn fibers and H_2SO_4-drawn + immersed fibers had a much higher increase in the degree of crystallinity reaching values in the range of 83–86%. These results are consistent with the removal of a large fraction of the amorphous PSS phase from the fibers, leaving behind a crystalline phase of PEDOT.

3.5. Electrical and mechanical properties of the fibers

Fig. 3a shows the electrical conductivity of raw fibers, DMSO-drawn fibers, H_2SO_4-drawn fibers, and H_2SO_4-drawn + immersed fibers, as a function of the draw ratio. Raw fibers had electrical conductivities as high as 1207 ± 94 S cm^{-1}. DMSO drawing enhanced the electrical conductivity to values as high as 2244 ± 83 S cm^{-1}, while sulfuric acid drawing enhanced it to values as high as 3663 ± 326 S cm^{-1}. In all cases, there was a slight increasing trend in conductivity with increased total draw. Moreover, the H_2SO_4-drawn + immersed sample reached a maximum value of 4039 ± 215 S cm^{-1}, which is the highest reported to date for a PEDOT:PSS fiber and is very close to the highest reported for a PEDOT:PSS film (4380 S cm^{-1}).[35] These enhancements are due to the combined effects of PSS removal, increased crystallite sizes and overall crystallinity, reduction of the (100) lamella stacking distance, and preferential orientation of the PEDOT chains in the fiber axis direction. Both the shortening of the (100) stacking distance and the improved crystallinity enhance the transport of charge carriers by promoting charge carrier delocalization and increasing their mean free path, thus, increasing their mobility and, therefore, the electrical conductivity. Correspondingly, Petsagkourakis *et al.*[50] recently reported an almost linear increase in charge carrier mobility with increasing crystallinity in PEDOT:Tosylate thin films. Furthermore, the mechanical drawing that the fibers experience results in the preferential orientation of the PEDOT chains in the fiber axis direction as inferred from the appearance of arcs in the 2D WAXS patterns (Fig. 2a–d). To quantify the degree of orientation, the (100) Hermans orientation factors, f_{100}, were calculated[51] (for more details see the ESI†). Raw fibers were weakly oriented with f_{100} values around 0.30. However, after drawing the fibers in DMSO or sulfuric acid, significant preferred orientation of the polymer chains was induced in the fiber axis direction, and f_{100} increased to values around 0.70 in both cases. Since charge transport is the fastest along the conjugated polymer backbone,[46] the electrical conductivity increases with alignment of the polymer chains along the fiber axis.

The mechanical properties of the fibers were also studied. Fig. 3b–d show the elongation at break, Young's modulus, and break stress as a function of total draw for the different fiber samples. Raw fibers have the largest elongations at break and lowest moduli, characteristic of a weakly oriented polymeric material. The Young's modulus increased as the fibers were drawn in DMSO due to the increased degree of preferred orientation of the polymer chains. However, the increase was larger when the fibers were drawn in sulfuric acid, despite the similar degree of orientation in both samples ($f_{100} \sim 0.70$, in both cases). Interestingly, the elongation at break of DMSO-drawn and H_2SO_4-drawn fibers was similar, which supports that the increase in Young's modulus was not solely due to increased preferred orientation. Instead, as excess PSS was removed from the fibers, the amorphous phase of the fiber was also removed, and so the concentration of the crystalline, oriented PEDOT phase increases. PEDOT chains are stiffer than the PSS chains due to their conjugated nature, thus, increasing the Young's moduli of the fibers to values as high as 22 GPa. The higher Young's moduli combined with the similar elongations at break results in H_2SO_4-drawn fibers having the highest break stresses with values as high as 550 MPa, which is the highest reported to date for a PEDOT:PSS fiber. It must be noted that the H_2SO_4-drawn + immersed fibers showed inter-filament fusion and surface damage occurred during their unwinding. Consequentially, this sample showed the lowest elongation at break among all the sulfuric acid treated samples and the lowest Young's modulus and break stress (with a rather large standard deviation) most likely stemming from existing tearing damage on the tested specimens caused when the fused filaments were separated.

As listed in Fig. 3a and d, electrical conductivity and Young's modulus follow similar trends. Electrical and mechanical properties are strongly correlated in conducting polymers because they both are affected by inter- and intrachain interactions.[19] Here, the electrical conductivity shows an almost linear increase with increasing Young's modulus as observed in Fig. 3e. This correlation is not coincidental since the Young's modulus could be used as a combined proxy for the degree of orientation of the polymer chains, and the percentage of crystalline oriented PEDOT phase in the fibers. It must be noted here, that in general, there is a tendency of the elongation at break to decrease as the Young's modulus, tensile strength, and electrical conductivity increase. This tendency stems from the increased orientation of the PEDOT chains and removal of amorphous PSS as the fibers are drawn through DMSO or sulfuric acid. For some applications, a high value of elongation at break might be preferred over a high electrical

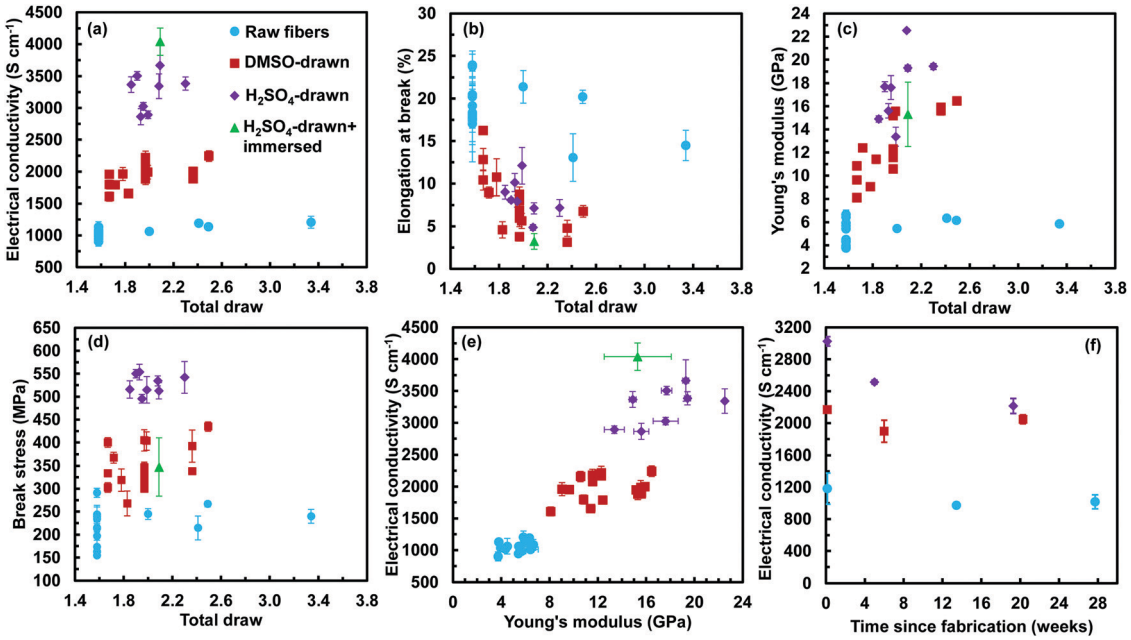

Fig. 3 (a) Electrical conductivity, (b) elongation at break, (c) Young's modulus, and (d) break stress of the fibers as a function of total draw. (e) Plot showing the correlation between electrical conductivity and Young's modulus. (f) Electrical conductivity of three representative samples as a function of the time since fabrication.

conductivity, in which case raw fibers might be used. On the contrary, if the fibers must withstand high levels of tensile stress and/or low resistance of the fibers is a priority, then drawn fibers are a better choice.

For comparison purposes, a summary of electrical and mechanical properties of wet-spun PEDOT:PSS fibers reported in the recent literature is included in Table 3.

3.6. Time stability of the electrical conductivity of the different PEDOT:PSS fibers

An important aspect to consider from the application perspective of the fibers, one that is often disregarded in the literature, is the time stability of their electrical properties. For the purpose of studying the stability, the electrical conductivity of three different samples was measured on different days after fabrication. The spools of fiber were kept in laboratory atmosphere (~21 °C and non-controlled relative humidity that ranged between 10–50%). Fig. 3f shows the values of electrical conductivity measured as a function of time since fabrication. The electrical conductivity of raw fibers and DMSO-drawn fibers remained almost unchanged (very slight decrease) 28 and 21 weeks after fabrication, respectively. However, the H_2SO_4-drawn fibers experienced degradation in their electrical properties, with a ~27% decrease in electrical conductivity

Table 3 Summary of electrical and mechanical properties of wet-spun PEDOT:PSS fibers from recent literature

Coagulation bath	Post-coagulation drawing	Post-treatment	Electrical conductivity (S cm^{-1})	Young's modulus (GPa)	Elongation at break (%)	Tensile strength (MPa)	Ref.
Acetone	No	No	0.1	1.1	4.3	17.2	24
	No	3 min immersion in ethylene glycol	467	4	7.7	130	25
IPA	No	No	264	2.5	13.5	97	26
50 vol% IPA in Acetone	Hot air	60 min immersion in ethylene glycol	2804	8.3	21	409.8	27
Concentrated H_2SO_4	No	No	968.4	>1.3	—	>100	31
	No	No	3828	3.9	36	425	29
	No	No	830	1.9	40	225	32
10 vol% DMSO in IPA	No	No	1207	4–6	17–22	150–250	This work
	DMSO	No	2244	16	5	400	
	Conc. H_2SO_4	No	3663	20–22	7.5	500–550	
	Conc. H_2SO_4	30 min immersion in conc. H_2SO_4	4039	15	3.2	350	

20 weeks after fabrication, with the electrical conductivity of the H_2SO_4-drawn fibers approaching that of the DMSO-drawn fibers. In view of these results, we can conclude that raw fibers and DMSO-drawn fibers present good stability with only a slight decrease in electrical conductivity after fabrication. On the other hand, the sulfuric acid fibers experienced a significant degradation. We believe this was due to mechanisms such as corrosion of electrical contacts and/or increased hygroscopicity due to sulfuric acid remaining in the fibers after treatment, or the possibility that the changes in the PEDOT structure after the sulfuric acid treatment are metastable. However, we cannot definitively corroborate any of these hypotheses and research in this area is ongoing.

Due to the stability issues of the H_2SO_4-drawn fibers, we chose to study the applications of the PEDOT:PSS fibers, presented in the next section, using the DMSO-drawn fibers due to their excellent long-term stability.

3.7. Applications of PEDOT:PSS fibers in electronic textiles

Future electronic textile devices will need flexible interconnections for power supply and communication between components. An important characteristic to consider for an interconnection is the maximum current carrying capacity or ampacity. Here, we define ampacity as the maximum current density that causes the immediate electrical failure of the conductor. The ampacity of raw fibers, DMSO-drawn fibers and H_2SO_4-drawn fibers was measured at 11.3, 18.1, and 21.1 kA cm^{-2}, respectively (Fig. S3, see ESI,† for more details). A similar value of ampacity (18 kA cm^{-2}) has been reported for PEDOT:PSS fibers fabricated by a two-step wet-spinning process where the fibers were first spun into IPA/acetone coagulation bath and then immersed for 1 h in ethylene glycol.[28] These values of ampacity are much higher than those typically found for PEDOT:PSS-coated textiles[52] and similar to typical ampacity values obtained for oriented carbon nanotube yarns (10–100 kA cm^{-2}).[53,54] These results indicate that the PEDOT:PSS fibers are strong candidates to be used as electrical interconnections. As a proof of concept, two bundles of 3 DMSO-drawn fibers were woven into a cotton cloth and connected to a red LED. As shown in Fig. 4a, the LED could be lit by passing 1 mA of current through the PEDOT:PSS fiber interconnections. Moreover, the interconnections remained functional even after continuous manipulation and bending (Fig. 4b).

Electrically conductive fibers, such as the PEDOT:PSS fibers fabricated in this work, are also great candidates to be used as the heating elements in textile heaters (see Fig. S4, ESI†).[28] A perhaps less evident potential application related to Joule

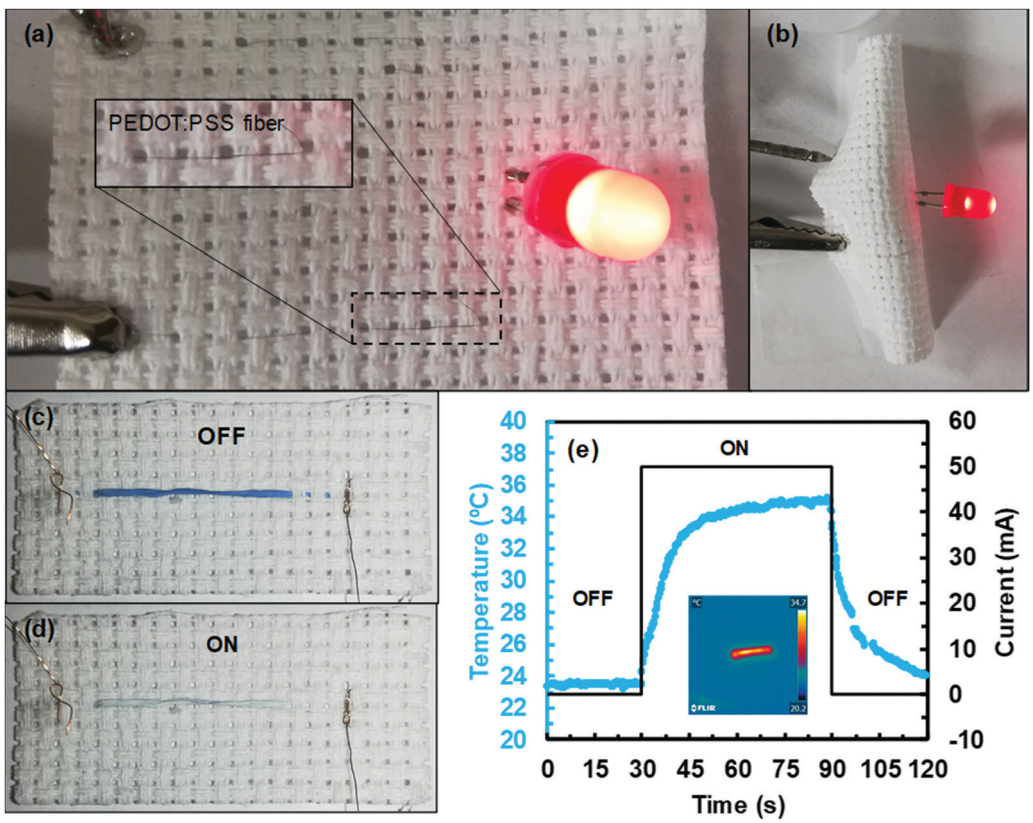

Fig. 4 (a) Photograph showing a red LED being lit by passing 1 mA through PEDOT:PSS fiber interconnections woven into cotton cloth. Inset shows an enlargement of a section of the PEDOT:PSS fibers. (b) Photographs showing functional interconnections even after bending the cotton cloth. Thermochromic PEDOT:PSS fiber bundle woven into a cotton cloth in its (c) OFF (blue) and (d) ON (white) state. (e) Temperature response of the bundle to a step change in current (inset: infrared image of the thermochromic bundle in its ON state).

heating is thermochromic textiles. Thermochromism is the property of changing color due to a change in temperature. To illustrate, a thermochromic PEDOT:PSS fiber bundle was fabricated by coating the bundle with a thermochromic paint that changed color from blue to white at 31 °C. Fig. 4c and d show the bundle woven into a cotton cloth in its OFF and ON state, respectively, where the color change from blue to white is clear (see also ESI†). The temperature of the bundle was raised above 31 °C by passing a current of 50 mA through the fibers as shown in Fig. 4e. These results demonstrated the potential of the PEDOT:PSS fibers to be used in on-demand color-changing clothing for fashion, camouflage purposes or even visual communication systems.

PEDOT-based materials have also shown very promising thermoelectric performance among polymer-based flexible thermoelectric materials.[55,56] Therefore, PEDOT:PSS fibers are ideal candidates as p-type legs in future textile thermoelectric generators (see Fig. S5, ESI†). As proof of concept, a thermoelectric textile device with 20 couples was built by weaving PEDOT:PSS fiber bundles in a cotton cloth as p-type legs while using alumel wire as n-type legs (see Fig. 5a). In this device, the DMSO-drawn fibers had a Seebeck coefficient, α, of $\sim$15 μV K^{-1} and a thermoelectric power factor, $\alpha^2\sigma$, of $\sim$50 μW m^{-1} K^{-2}. The output characteristics of the device are shown in Fig. 5b. A maximum output power of $\sim$2.82 μW was achieved at a ΔT of 84 °C. A fabric made from these PEDOT:PSS fibers could be made to be wrapped onto hot objects such as exhaust or steam pipes where a temperature gradient around 80 °C is plausible. In the case of wearable textiles, a much lower ΔT (5 to 30 °C) is to be expected. The maximum output power is plotted as a function of ΔT in Fig. 5c showing a parabolic trend with increasing ΔT in accordance with eqn (S14) (ESI†). Additionally, the inset in Fig. 5c zooms into the low ΔT portion of the curve showing output powers from 20 to 250 nW in the 5 to 30 °C ΔT range. It must be noted that the textile thermoelectric generator fabricated in this work is not optimized, but is quite comparable to other devices in the literature (see Table S1, ESI†), having one of the highest power outputs reported for a textile thermoelectric device. This is due to the high power factor of the PEDOT:PSS fibers (p-type material) compared to the other PEDOT:PSS-based textile materials, second only to carbon nanotube-based textile materials. As stated earlier, we used DMSO-drawn fibers to fabricate the device due to the stability issues of the H_2SO_4-drawn fibers, however, fresh H_2SO_4-drawn fibers have a superior thermoelectric performance with a Seebeck coefficient around 18–19 μV K^{-1} and a power factor of $\sim$115 μW m^{-1} K^{-2}, which, to the best of our knowledge, is the highest reported for a PEDOT:PSS fiber. Therefore, the performance of these PEDOT:PSS fiber-based thermoelectric devices could be enhanced by using the H_2SO_4-drawn fibers if stability issues are solved. Moreover, miniaturization and further optimization of other device parameters should further lead to much higher power outputs at lower ΔT.

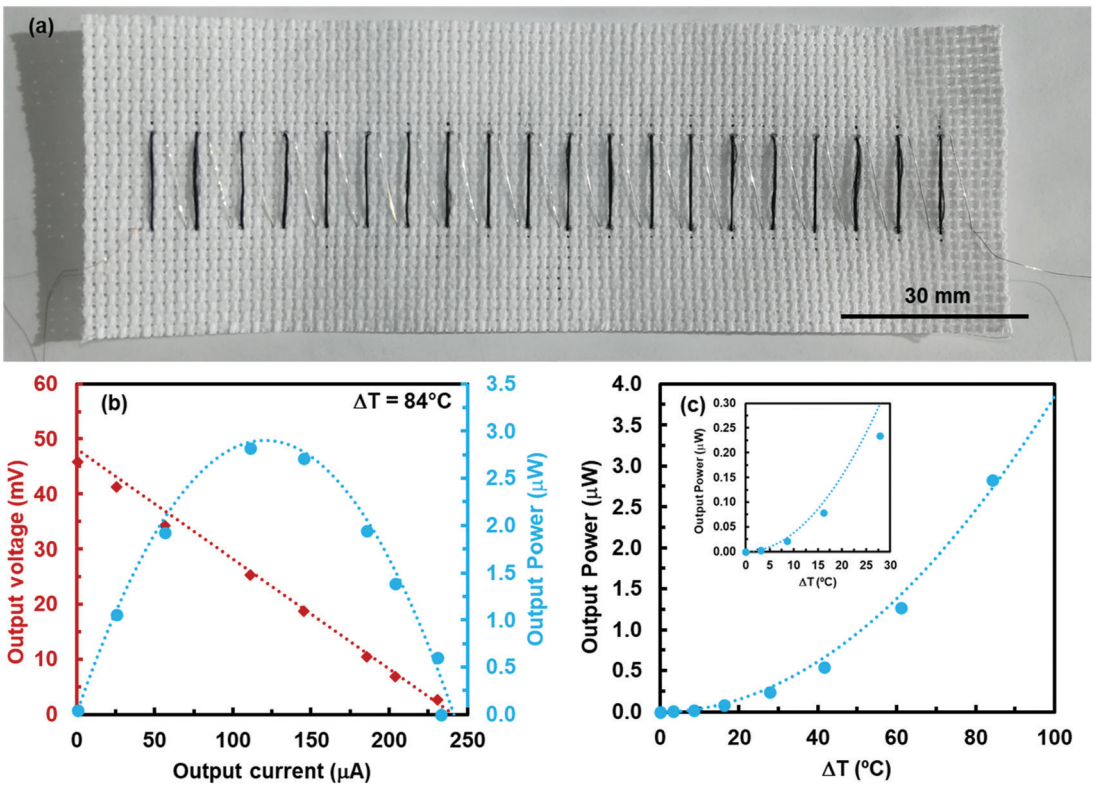

Fig. 5 (a) Photograph of the textile thermoelectric device fabricated by stitching PEDOT:PSS fiber bundles and alumel wire to a cotton cloth. (b) Output characteristics of the device as a function of the output current at ΔT = 84 °C. (c) Output power of the device as a function of ΔT. Inset: Zoom to the lower ΔT portion of the output power curve. The dotted curves in (b) and (c) represent the theoretical fit to eqn (S9), (S12) and (S14) (ESI†).

Finally, we also explored the use of the PEDOT:PSS fibers as the channel in organic electrochemical transistors (OECTs) (see Fig. S6a, ESI†). Fig. 6a shows a photograph of an OECT fabricated using one DMSO-drawn PEDOT:PSS fiber as the channel, copper wire as the gate and a polyvinyl alcohol/phosphoric acid solid electrolyte. PEDOT:PSS-based OECTs are conductive when the gate voltage, V_G, is zero and become less conductive at positive non-zero gate voltages (p-type depletion mode OECTs).[57–59] In Fig. 6b, the output curves are plotted to show the dependence of the drain current, I_D, on the drain voltage, V_D, for different V_G from 0 to 0.7 V. At low values of V_D, the current shows a linear dependence on V_D, however, the current saturates at higher voltages. Additionally, as V_G is increased the drain current decreases. The decrease in current when increasing V_G is caused by the dedoping of the PEDOT in the fiber channel; cations from the electrolyte are injected into the channel, which neutralize the negative charges of the counterion (PSS) and the PEDOT chains are dedoped, resulting in the reduction of the channel electrical conductivity, effectively decreasing the drain current. From an electronic circuit point of view, the OECT behaves as a variable resistor or switch, where the resistance of the PEDOT:PSS fiber acting as channel can be varied by applying a gate voltage. To demonstrate some of the capabilities of these devices in electronic textiles, a dimmer was built for an LED that was attached to a cotton cloth with electrical interconnections made of PEDOT:PSS fibers. This simple dimmer was made by attaching copper wire to the cotton cloth and depositing the solid electrolyte covering part of the copper wire (gate) and a section of the PEDOT:PSS fiber interconnection. That section of the PEDOT:PSS interconnection acted as the OECT channel and its resistance could be modulated by applying a voltage to the gate, effectively modulating the current applied to the LED. Fig. 6c shows a photograph of the OECT dimmer, LED, and interconnections on the cotton cloth, including a schematic representation of the applied voltages. Fig. 6d shows the LED emitting light at different intensities from more intense at $V_G = 0$ to completely off at $V_G = 1$ V, while applying a constant drain voltage of −3.3 V.

OECTs can also be used as signal amplifiers, whereby small input signals (gate voltage) are transduced into large changes in an output signal (drain current). This is one of the reasons OECTs are widely used as biosensors, where input signals can be in the order of mV or μV.[60] The signal transduction is characterized by the transfer curves that describe the dependence of I_D on V_G, and the transduction efficiency is usually

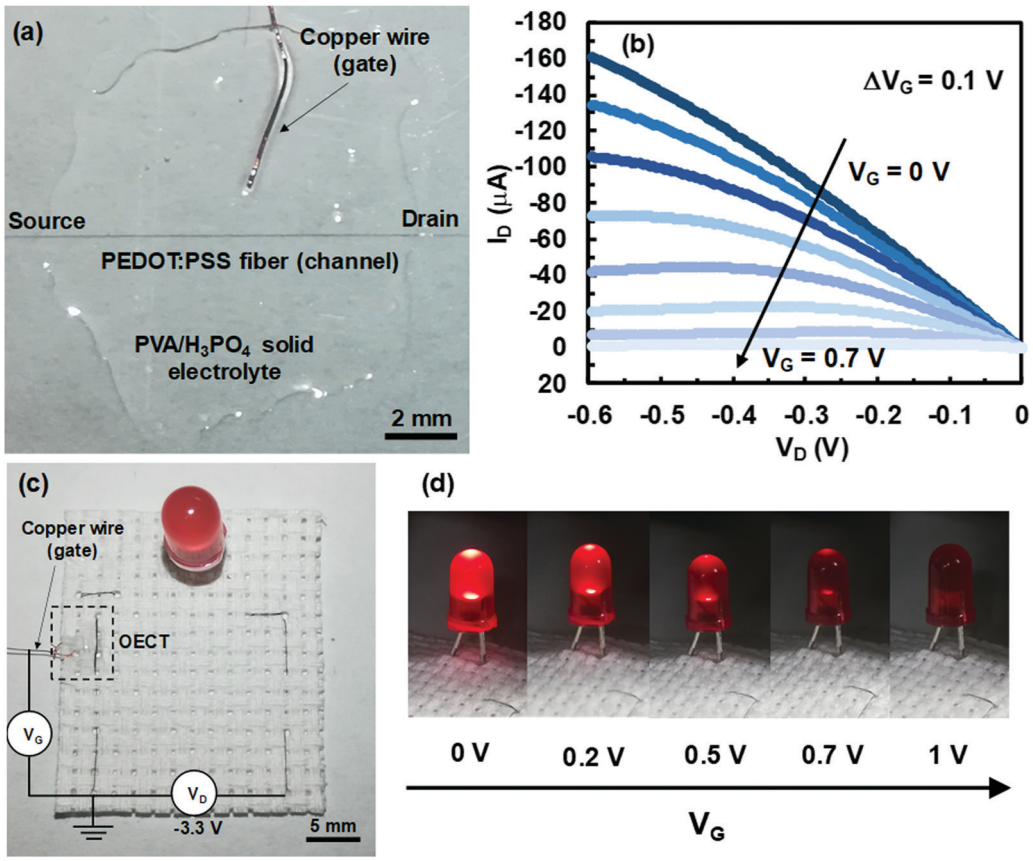

Fig. 6 (a) Photograph of the PEDOT:PSS fiber-based OECT. (b) Output curves showing the dependence of I_D on V_D at different V_G from 0 to 0.7 V with ΔV_G of 0.1 V and channel length of 1 cm. (c) Photograph of an LED attached to a cotton cloth with PEDOT:PSS sewn fiber interconnections with dimming capabilities by including a PEDOT:PSS fiber-based OECT. (d) Photographs showing the LED emitting light at different intensities by changing the gate voltage from 0 V to 1 V while applying a constant drain voltage of −3.3 V.

calculated using the first derivative of these transfer curves, called transconductance, g_m (eqn (S15), ESI†).[57] Typical values of transconductance for OECTs in film geometry are in the order of mS. The OECT fabricated here (Fig. 6a), using only 1 fiber as the channel, had a maximum transconductance of 314 μS (Fig. S6b and c, ESI†), an order of magnitude lower than typical PEDOT:PSS-based OECTs in the film geometry. Nevertheless, the transconductance can be increased by fabricating OECTs with more fibers connected in parallel acting as the channel (Fig. S6d–e, ESI†). By using 10 fibers as the channel, the maximum transconductance increased to around 4 mS. The transconductance of these PEDOT:PSS fiber-based OECTs could be further increased by using bundles with even more fibers as the channel or by reducing the channel length. Nevertheless, the unoptimized values reported here are on the same order as those of typical OECTs in the film geometry. This suggest that textile PEDOT:PSS fiber-based OECTs could be used in the future to record biological signals, such as heart or brain activity, in wearable health monitoring textile devices.

4. Conclusions

Conjugated polymer fibers are promising candidates for use as building blocks in the emerging field of electronic textiles. In this work, we explored the use of sulfuric acid as a drawing media and compared it to the use of DMSO during the fabrication of highly conductive PEDOT:PSS fibers. Sulfuric acid drawing was proven very effective at improving the PEDOT:PSS fibers' properties. H_2SO_4-drawn fibers showed outstanding electrical conductivities with values as high as 3663 ± 326 S cm^{-1}. Moreover, the mechanical properties of the fibers were also enhanced, with Young's modulus and break stress values as high as 22 GPa and 550 MPa, respectively. Additionally, the electrical conductivity of these fibers was further increased to 4039 ± 215 S cm^{-1} by immersing the fibers in sulfuric acid for additional time. The improvement of the electrical and mechanical properties was explained in terms of changes in the composition and structure of the fibers after the sulfuric acid treatment. In short, the sulfuric acid drawing step removed excess PSS from the fibers while also promoting the ion exchange of sulfates in place of PSS as counterions, resulting in crystal reorganization of the PEDOT, reduced (100) lamella stacking distance, and overall increased crystallinity. However, the electrical conductivity of the H_2SO_4-drawn fibers was unstable with time, which contrasted with the excellent stability of the DMSO-drawn fibers.

Additionally, the use of the PEDOT:PSS fibers in multiple electronic textile applications was demonstrated. Proof of concept devices were fabricated by sewing the fibers in a cotton cloth, demonstrating the fibers capabilities to be used as flexible interconnections, in on-demand color-switching thermochromic textiles, as p-type legs in textile thermoelectric generators, and as the channel in a fiber-based organic electrochemical transistor. The PEDOT:PSS fibers fabricated in this work are a unique type of material with the potential of becoming a cornerstone in the emerging field of electronic textiles.

Conflicts of interest

There are no conflicts of interest to declare.

Acknowledgements

This material is based upon work supported by the National Science Foundation under Cooperative Agreement No. 1849213. Any opinions, findings, and conclusions or recommendations expressed in this material are those of the authors and do not necessarily reflect the views of the National Science Foundation.

References

1 B. L. Hardy, M. H. Moncel, C. Kerfant, M. Lebon, L. Bellot-Gurlet and N. Mélard, *Sci. Rep.*, 2020, **10**, 4889.
2 J. M. Adovasio, O. Soffer and B. Klíma, *Antiquity*, 2015, **70**, 526–534.
3 M.-N. Nashed, D. A. Hardy, T. Hughes-Riley and T. Dias, *Fibers*, 2019, **7**, 12.
4 Y. Xia and L. Yun, *Compos. Sci. Technol.*, 2008, **68**, 1471–1479.
5 A. Varesano, A. Belluati, D. O. Sanchez Ramirez, R. A. Carletto, C. Vineis, C. Tonetti, M. Bianchetto Songia and G. Mazzuchetti, *J. Appl. Polym. Sci.*, 2016, **133**, 42831.
6 S. Garg, C. Hurren and A. Kaynak, *Synth. Met.*, 2007, **157**, 41–47.
7 J. Molina, J. Fernández, A. I. del Río, R. Lapuente, J. Bonastre and F. Cases, *Polym. Degrad. Stab.*, 2010, **95**, 2574–2583.
8 S. W. Finefrock, X. Zhu, Y. Sun and Y. Wu, *Nanoscale*, 2015, **7**, 5598–5602.
9 Y. Du, K. Cai, S. Chen, H. Wang, S. Z. Shen, R. Donelson and T. Lin, *Sci. Rep.*, 2015, **5**, 6411.
10 K. Kirihara, Q. Wei, M. Mukaida and T. Ishida, *Synth. Met.*, 2017, **225**, 41–48.
11 J. D. Ryan, D. A. Mengistie, R. Gabrielsson, A. Lund and C. Müller, *ACS Appl. Mater. Interfaces*, 2017, **9**, 9045–9050.
12 A. Lund, S. Darabi, S. Hultmark, J. D. Ryan, B. Andersson, A. Ström and C. Müller, *Adv. Mater. Technol.*, 2018, **3**, 1800251.
13 A. Lund, N. M. van der Velden, N.-K. Persson, M. M. Hamedi and C. Müller, *Mater. Sci. Eng., R*, 2018, **126**, 1–29.
14 A. G. MacDiarmid and A. J. Epstein, *Faraday Discuss. Chem. Soc.*, 1989, **88**, 317–332.
15 J. E. Fischer, X. Tang, E. M. Scherr, V. B. Cajipe and A. G. MacDiarmid, *Synth. Met.*, 1991, **41**, 661–664.
16 B. R. Mattes, H. L. Wang, D. Yang, Y. T. Zhua, W. R. Blumenthala and M. F. Hundleya, *Synth. Met.*, 1997, **84**, 45–49.

17 S. J. Pomfret, P. N. Adams, N. P. Comfort and A. P. Monkman, *Polymer*, 2000, **41**, 2265–2269.
18 J. Moulton and P. Smith, *Synth. Met.*, 1991, **40**, 13–22.
19 J. Moulton and P. Smith, *Polymer*, 1992, **33**, 2340–2347.
20 J. Fanous, M. Schweizer, D. Schawaller and M. R. Buchmeiser, *Macromol. Mater. Eng.*, 2012, **297**, 123–127.
21 J. Foroughi, G. M. Spinks, G. G. Wallace and P. G. Whitten, *Synth. Met.*, 2008, **158**, 104–107.
22 J. Foroughi, G. M. Spinks and G. G. Wallace, *Synth. Met.*, 2009, **159**, 1837–1843.
23 J. Foroughi, S. R. Ghorbani, G. Peleckis, G. M. Spinks, G. G. Wallace, X. L. Wang and S. X. Dou, *J. Appl. Phys.*, 2010, **107**, 103712.
24 H. Okuzaki and M. Ishihara, *Macromol. Rapid Commun.*, 2003, **24**, 261–264.
25 H. Okuzaki, Y. Harashina and H. Yan, *Eur. Polym. J.*, 2009, **45**, 256–261.
26 R. Jalili, J. M. Razal, P. C. Innis and G. G. Wallace, *Adv. Funct. Mater.*, 2011, **21**, 3363–3370.
27 J. Zhou, E. Q. Li, R. Li, X. Xu, I. A. Ventura, A. Moussawi, D. H. Anjum, M. N. Hedhili, D.-M. Smilgies, G. Lubineau and S. T. Thoroddsen, *J. Mater. Chem. C*, 2015, **3**, 2528–2538.
28 J. Zhou, M. Mulle, Y. Zhang, X. Xu, E. Q. Li, F. Han, S. T. Thoroddsen and G. Lubineau, *J. Mater. Chem. C*, 2016, **4**, 1238–1249.
29 J. Zhang, S. Seyedin, S. Qin, P. Lynch, Z. Wang, W. Yang, X. Wang and J. Razal, *J. Mater. Chem. A*, 2019, **7**, 6401–6410.
30 R. Sarabia-Riquelme, M. Shahi, J. W. Brill and M. C. Weisenberger, *ACS Appl. Polym. Mater.*, 2019, **1**, 2157–2167.
31 Y. Kim, T. Lim, C.-H. Kim, C. S. Yeo, K. Seo, S.-M. Kim, J. Kim, S. Y. Park, S. Ju and M.-H. Yoon, *NPG Asia Mater.*, 2018, **10**, 1086–1095.
32 Y. Kim, A. Lund, H. Noh, A. I. Hofmann, M. Craighero, S. Darabi, S. Zokaei, J. I. Park, M.-H. Yoon and C. Müller, *Macromol. Mater. Eng.*, 2020, **305**, 1900749.
33 Y. Xia and J. Ouyang, *ACS Appl. Mater. Interfaces*, 2010, **2**, 474–483.
34 Y. Xia, K. Sun and J. Ouyang, *Adv. Mater.*, 2012, **24**, 2436–2440.
35 N. Kim, S. Kee, S. H. Lee, B. H. Lee, Y. H. Kahng, Y.-R. Jo, B.-J. Kim and K. Lee, *Adv. Mater.*, 2014, **26**, 2268–2272.
36 M. N. Gueye, A. Carella, N. Massonnet, E. Yvenou, S. Brenet, J. Faure-Vincent, S. Pouget, F. Rieutord, H. Okuno, A. Benayad, R. Demadrille and J.-P. Simonato, *Chem. Mater.*, 2016, **28**, 3462–3468.
37 Z. U. Khan, O. Bubnova, M. J. Jafari, R. Brooke, X. Liu, R. Gabrielsson, T. Ederth, D. R. Evans, J. W. Andreasen, M. Fahlman and X. Crispin, *J. Mater. Chem. C*, 2015, **3**, 10616–10623.
38 A. V. Shchukarev and D. V. Korolkov, *Cent. Eur. J. Chem.*, 2004, **2**, 347–362.
39 Z. D. Hood, S. P. Adhikari, S. F. Evans, H. Wang, Y. Li, A. K. Naskar, M. Chi, A. Lachgar and M. P. Paranthaman, *Carbon Resour. Convers.*, 2018, **1**, 165–173.
40 X. Crispin, S. Marciniak, W. Osikowicz, G. Zotti, A. W. D. van der Gon, F. Louwet, M. Fahlman, L. Groenendaal, F. De Schryver and W. R. Salaneck, *J. Polym. Sci., Part B: Polym. Phys.*, 2003, **41**, 2561–2583.
41 X. Hu, G. Chen, X. Wang and H. Wang, *J. Mater. Chem. A*, 2015, **3**, 20896–20902.
42 A. Dkhissi, D. Beljonne, R. Lazzaroni, F. Louwet, L. Groenendaal and J. L. Brédas, *Int. J. Quantum Chem.*, 2003, **91**, 517–523.
43 K. Siow, L. Britcher, S. Kumar and H. Griesser, *Sains Malays.*, 2018, **47**, 1913–1922.
44 T. Takano, H. Masunaga, A. Fujiwara, H. Okuzaki and T. Sasaki, *Macromolecules*, 2012, **45**, 3859–3865.
45 Q. Wei, M. Mukaida, Y. Naitoh and T. Ishida, *Adv. Mater.*, 2013, **25**, 2831–2836.
46 K. E. Aasmundtveit, E. J. Samuelsen, L. A. A. Pettersson, O. Inganäs, T. Johansson and R. Feidenhans'l, *Synth. Met.*, 1999, **101**, 561–564.
47 N. Massonnet, A. Carella, A. de Geyer, J. Faure-Vincent and J.-P. Simonato, *Chem. Sci.*, 2015, **6**, 412–417.
48 N. Kim, B. H. Lee, D. Choi, G. Kim, H. Kim, J.-R. Kim, J. Lee, Y. H. Kahng and K. Lee, *Phys. Rev. Lett.*, 2012, **109**, 106405.
49 D. Farka, A. O. F. Jones, R. Menon, N. S. Sariciftci and P. Stadler, *Synth. Met.*, 2018, **240**, 59–66.
50 I. Petsagkourakis, E. Pavlopoulou, E. Cloutet, Y. F. Chen, X. Liu, M. Fahlman, M. Berggren, X. Crispin, S. Dilhaire, G. Fleury and G. Hadziioannou, *Org. Electron.*, 2018, **52**, 335–341.
51 H. H. Chuah and B. T. A. Chang, *Polym. Bull.*, 2001, **46**, 307–313.
52 M. T. Otley, F. A. Alamer, Y. Guo, J. Santana, E. Eren, M. Li, J. Lombardi and G. A. Sotzing, *Macromol. Mater. Eng.*, 2017, **302**, 1600348.
53 A. Lekawa-Raus, J. Patmore, L. Kurzepa, J. Bulmer and K. Koziol, *Adv. Funct. Mater.*, 2014, **24**, 3661–3682.
54 G. Mokry, J. Pozuelo, J. J. Vilatela, J. Sanz and J. Baselga, *Nanomaterials*, 2019, **9**, 383.
55 K. Sun, S. Zhang, P. Li, Y. Xia, X. Zhang, D. Du, F. Isikgor and J. Ouyang, *J. Mater. Sci.: Mater. Electron.*, 2015, **26**, 1–25.
56 R. Kroon, D. A. Mengistie, D. Kiefer, J. Hynynen, J. D. Ryan, L. Yu and C. Müller, *Chem. Soc. Rev.*, 2016, **45**, 6147–6164.
57 J. Rivnay, S. Inal, A. Salleo, R. M. Owens, M. Berggren and G. G. Malliaras, *Nat. Rev. Mater.*, 2018, **3**, 17086.
58 H. S. White, G. P. Kittlesen and M. S. Wrighton, *J. Am. Chem. Soc.*, 1984, **106**, 5375–5377.
59 S.-M. Kim, C.-H. Kim, Y. Kim, N. Kim, W.-J. Lee, E.-H. Lee, D. Kim, S. Park, K. Lee, J. Rivnay and M.-H. Yoon, *Nat. Commun.*, 2018, **9**, 3858.
60 M. Braendlein, T. Lonjaret, P. Leleux, J.-M. Badier and G. G. Malliaras, *Adv. Sci.*, 2017, **4**, 1600247.